ACS OMEGA

http://pubs.acs.org/journal/acsodf

Article

Development and Characterization of Natural Chromite Coating on Metal Substrate Using the Plasma Spray Process

Zeeshan Ahmad Abbasi, Abdul Mateen, Akbar Niaz,* Muhammad Atiq Ur Rehman,* and Abdul Wadood

Cite This: *ACS Omega* 2023, 8, 15193−15202

Read Online

ACCESS | Metrics & More | Article Recommendations

ABSTRACT: Natural materials are gaining interest as coating feedstock because their "quality to cost" ratio is better and they are more environmentally friendly than most of the synthetic ceramics. They give sufficient protection to metal surfaces against harsh conditions such as corrosion, wear, and high temperature. In the current study, chromite mineral was beneficiated and reduced to two different sizes to be used as feedstock material for thermal spray coating. Powders were upgraded by gravity and magnetic separation, respectively, and thermally sprayed onto mild steel samples by using atmospheric plasma spray (APS) equipment. Morphology, structure, phases, elemental distribution of chromite powder, and coatings were studied using field emission scanning electron microscopy, X-ray diffraction, X-ray fluorescence spectroscopy, and energy-dispersive X-ray spectroscopy. Tribological properties of APS chromite coatings were investigated by using a ball-on-disk tribometer, and corrosion resistance properties were evaluated by carrying out potentiodynamic polarization testing in 3.5% NaCl solution. It is observed that the coating has better wear and corrosion resistance and is worn by abrasive wear that includes scratching and particles pull out. Coating efficiency, surface morphology, and microhardness of the coating developed by fine powder were better than those of coarse powder coating.

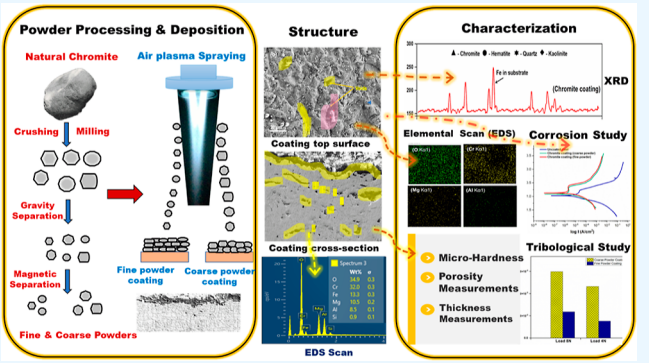

1. INTRODUCTION

Natural materials are gaining tremendous attention due to their sustainability, cost effectiveness, non-carcinogenic nature, and ecological compatibility. Various natural ores, minerals, and mine wastes have been thermally sprayed recently onto metal substrates to achieve desired properties like corrosion, thermal, electrical, and wear resistance.[1−5] Some of the materials used in these coatings were ilmenite, garnet, olivine, hydroxyapatite, and basalt.[6,7] Natural materials such as diopside, forsterite, and tourmaline were studied as an alternative to ceramic type materials for electrical, thermal, and wear resistance properties.[1,8,9] Ceramics and minerals both have the ability to withstand their integrity at elevated pressure and temperatures; therefore, they can be used in harsh environmental conditions due to their sustainability and high melting temperatures.[10] Thermal spray method like atmospheric plasma spraying (APS) has been extensively used to study high melting temperature materials such as ceramics and minerals.[7,11−13] APS can generate temperature up to 15,000 °C and this technique is best suited for materials with higher melting points as it gives higher particle temperature as compared to others, which result in a thicker coating on the substrate.[14,15] Particle temperature in APS depend on certain parameters like feeding rate of particles, distance of substrate from gun, particles size and distribution, and so forth. Both particle temperature and velocity at impact are strongly dependent on starting powder particle size and morphology.[16] Moreover, the in-flight behavior of different particle sizes is known to play a crucial role in affecting the coating properties.[17,18]

Chromite mineral is extensively used for the extraction of chromium metal and in ferroalloys industry. General formula given is (Mg, Fe)O. $(Cr, Al, Fe)_2O_3$.[19] Chromite is found in the form of ultramafic igneous rocks with some unwanted associated gangue minerals.[20] Main oxides present in natural chromite are that of chromium (Cr_2O_3), iron (Fe_2O_3), magnesium (MgO), aluminum (Al_2O_3), and silicon (SiO_2), whereas chromite having greater than 45% chromium oxide (Cr_2O_3) is considered as a high-grade chrome ore.[21] Chromite

Received: January 10, 2023
Accepted: April 4, 2023
Published: April 18, 2023

mineral does not have specific a melting point rather a range of melting temperatures due to the difference in oxide compositions; chromite mineral has a melting temperature range of 1850−2200 °C.[22,23] Some of the gangue minerals found along with chromite are silicates and aluminates, such as olivine, kaolinite, and quartz mineral.[24] Beneficiation is required for further processing of chromite mineral, which involves comminution and concentration.[25] Chromium oxide (Cr_2O_3) that is one of the constituent of chromite has been extensively studied as a coating material for thermal protection, wear resistance, and refractory applications.[26−29] Thin chromite coating has been produced in past with HVOF technique which shows good corrosion resistance and adequate wear resistance but coating thickness was very low (20 μm) due to temperature limitation in the HVOF technique.[30] APS-sprayed Cr_2O_3 coatings give better corrosion resistance to metal substrate due to the formation of a passive film on the surface.[31,32]

Processing and recycling of commercially available synthetic materials create biohazard waste that is undesirable; therefore, emphasis has been done to utilize natural materials as coating feedstock. There are many investigations performed to use natural feedstock materials for plasma spray coatings, but no effort was made for plasma spray coating of natural chromite. When natural chromite rock was ground and upgraded, it can be used as a coating feedstock for plasma spraying. The aim of the present research is to examine the usefulness of chromite as coating feedstock powder for plasma spraying on steel substrate and to study as-sprayed coatings for their tribological and corrosion resistance properties. Effect of particle size on coating properties was also studied. This study will provide an idea to technologists about the use of cost-effective natural materials, as an alternative to synthetic ceramics.

2. MATERIAL AND METHODS

2.1. Materials. The material used for coating process is chromite mineral. AISI 1018 mild carbon steel (mild steel) was used as a substrate metal. It has 0.17% carbon content in it and its measured value of hardness is 132 ± 7 HV at 30 kg load condition. In the first step, comminution and beneficiation of chromite was carried out that involves crushing, grinding, and milling actions to reduce the particle size. Beneficiation was then performed through gravity and magnetic separation processes to upgrade chromite by removing unwanted phases such as gangue mineral components. In the first step, the ore was converted into fine powder consisting of two particle sizes with a low gangue/earthly impurity. In the second step, these two powder sizes were utilized to deposit coatings using the APS technique.

2.2. Beneficiation and Comminution Process. Native lump of chromite was selected for crushing and grinding to obtain micrometer-sized fine feedstock powder for coating. Crushing was carried out using a jaw and roll crusher, respectively, to reach a size of 2 mm particles. A further reduction in size was achieved through grinding into a rod mill to achieve ≤50 μm size. One batch was further reduced to ≤20 μm by ball milling. The final sizes achieved are consisted of coarse powder (particles averaging 31−88 μm in size) and fine powder (8−48 μm in size), as analyzed by a particle analyzer.

The ore beneficiation process involves the removal of gangue mineral/earthly impurities from ore mineral through gravity and magnetic separation processes. Wilfley Shaking Table was used for gravity separation to remove gangue mineral as it is more economical and easier to exercise.[25] Further beneficiation is done by passing the particles through a Boxmag Magnetic Separator. During magnetic separation desirable chromite particles that are susceptible to magnetic field get deflected by permanent magnetic roller and collected on the inner side of the hopper.[33] The magnetic chromite particles make up a final upgraded feedstock powder, ready for spraying.

2.3. APS Deposition of Chromite Feedstock Powder. Equipment used for spraying was the Sulzer Metco Plasma Spray System with 9 MB spray gun. Mild steel samples with a cross-sectional dimension of 50 × 35 × 3 mm were grit blasted and used as substrates. The substrate surface was flushed with acetone and sonicated in water bath before measuring average surface roughness (Ra) by Mitutoyo Surftest equipment. The average surface roughness measured from 10 × 10 mm area for the steel samples was Ra 3.2 ± 0.2 μm. Powders were sprayed through the SX-03-2 powder feeder, and spraying conditions used are given in Table 1. Parameters for APS were optimized by changing the feed rates of fuel gases and powders until optimal coating was achieved. After optimizing, identical process parameters for both fine and coarse size particles were used to compare coating characteristics. Coated samples were allowed to cool at room temperature and then cut into smaller samples using an electrical discharge machine (EDM) for metallographic analysis.

Table 1. Plasma Spraying Parameters

coating parameter	value
plasma gun	9 MB
current (A)	400
voltage (V)	60
gas flow Argon (l/mijln)	45
gas flow Hydrogen (l/min)	12
spray distance (mm)	110
powder feed rate (g/min)	20

2.4. Structure and Phase Identification. Microstructure, chemical composition, and phase identification of chromite powder, before and after the coating of surfaces, were analyzed using field emission scanning electron microscopy (FESEM Mira Scan 3 TESCAN) with energy-dispersive spectroscopy (EDS) (Oxford Instruments), X-ray florescence spectroscopy (AxiosMet, Panalytical), and X-ray diffraction (XRD) equipment (GNR Analytical Instruments) with a Cu Kα radiation source.

2.5. Friction and Wear Test. A ball-on-disk tribometer (Microtest) was used for investigating the friction and wear characteristics of the coatings. Samples with dimensions of 15 × 15 × 3 mm were used as a disk in assembly where the disk is rotating and the ball is stationary. Coated samples were tested for wear resistance behavior at room temperature under dry conditions by using hardened 100Cr6 steel ball of 3 mm diameter as the counterbody. The steel substrate sample was polished for friction and wear tests (Ra 0.17 μm). Wear test parameters are shown in Table 2.

2.6. Microhardness and Porosity Measurements. Vickers microhardness tester was used to measure the hardness of coatings on polished sections. Load of 200 gf was applied for 15 s for hardness measurements. Mean value of microhardness from five indentations was calculated and reported for each coating. An optical microscope (SZ 61, Olympus) equipped

https://doi.org/10.1021/acsomega.3c00194
ACS Omega 2023, 8, 15193−15202

Table 2. Tribological Test Parameters on Plasma Sprayed Coatings

parameter	Value
applied load (N)	4, 8
revolution (rpm)	100
sliding distance (m)	50
wear track radius (mm)	7
atmosphere	Dry
temperature	26 ± 2°C
humidity	65 ± 5%

with digital camera (DP 25, Olympus) was used to collect micrographs for porosity measurement. Porosity was measured from the difference in gray levels due to variances in the intensity of reflected light from specimen. Porosity of each coating was analyzed from 10 images, from different areas through image analysis software (AnalySIS FIVE, Olympus).

2.7. Corrosion Test. Electrochemical corrosion test was performed on both coated and uncoated samples having a circular geometry of 16 mm diameter. Gamry Reference 600 Potentiostat, having three electrodes in a glass cell with 3.5% NaCl solution as the electrolyte, was used for potentiodynamic polarization measurements at a scan rate of 0.5 mV/s. Open circuit potential (OCP) reached to steady state after immersing the sample in electrolyte for 15 min and scanning range of potential was selected from −800 to +1250 mV with respect to OCP. Tests were performed at 26 ± 2 °C, samples were grinded with a mesh size of 1200 μm and cleaned ultrasonically before the experiment. In this setup, saturated calomel electrode (SCE) was used as the reference and platinum as the auxiliary electrode. Potentiodynamic polarization curves were drawn for substrate and coated samples. Tafel extrapolation of the polarization graphs was used to find the corrosion current density (I_{corr}) and corrosion potential (E_{corr}) for all the samples.

3. RESULTS AND DISCUSSION

3.1. Morphology, Microstructure, and Composition of the Powders. Morphology of both fine and coarse powders was the same and the only difference is their sizes (Figure 1). Micrographs and sieve analysis confirm that both fine and coarse powder were irregular in shape having range of particle sizes from 8 to 48 and 31 to 88 μm, respectively (Figure 2). Range of sizes with irregularity in shape helps

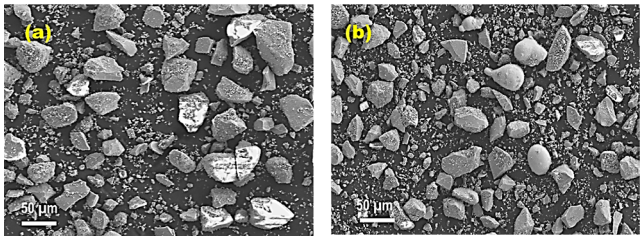

Figure 2. SEM images of coarse (a) and fine (b) chromite powder.

toward better adhesion on the surface during thermal spraying, and large irregular particles may be packed well with small particles on impact to the substrate surface, but there is also a chance of unmelted large particles on the coating surface.

Chemical composition of chromite powder determined by EDS and XRF is shown in Tables 3 and 4. Elemental analysis done by EDS in Table 3 shows oxygen (O) as a major element in powder due to the oxide nature of constituents, as evident from Table 4. Chromium oxide is above 50% which makes it metallurgical grade and significant amount of iron oxide makes it iron-rich chromite ore.[34,35] Oxides of magnesium and aluminum are also present in reasonable amounts, and based on composition, we can write the general chemical formula as (Mg, Fe)O. $(Cr, Al, Fe)_2O_3$.[36,37] A small amount of silica present in the sample is the main impurity associated with most chromite minerals.[38]

The XRD patterns of powders were obtained between 2θ ranges of 20−80° to identify the phases present in chromite powder (Figure 3). Diffraction peaks were analyzed using MDI JADE software and it was found that the peaks were consistent with the patterns for the chromite mineral.[24] Moreover, chromite peaks were distinctive and no broadening of the XRD patterns was observed, which shows the crystalline nature of the powder. X-ray diffractogram shows that chromite and hematite are two major phases present in the powder. Peaks corresponding to Quartz and kaolinite phases are also visible in

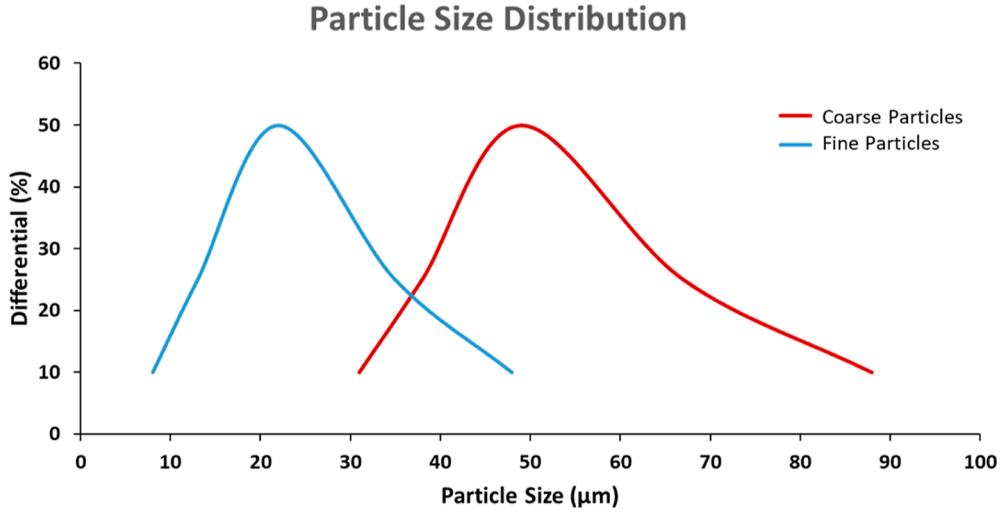

Figure 1. Particle size distribution curve.

https://doi.org/10.1021/acsomega.3c00194
ACS Omega 2023, 8, 15193−15202

Table 3. Chemical Analysis in Weight Percent (EDS) of Chromite Powder

elements by EDS	oxygen (O)	chromium (Cr)	iron (Fe)	magnesium (Mg)	aluminum (Al)	silicon (Si)
weight %	36.12	34.52	10.97	8.79	7.57	2.07

Table 4. Chemical Analysis in Weight Percent (XRF) of Chromite Powder

oxide content by XRF	Cr_2O_3	Fe_2O_3	MgO	Al_2O_3	SiO_2	LOI[a]
weight %	50.17	15.21	14.52	14.12	4.08	1.90

[a]Loss on ignition (LOI).

the pattern, and they coexist with chromite mineral as gangue materials.

3.2. Coating Characterization. XRD pattern of coating has been compared with that of powder and it has been found that the chromite phase has been retained in the coating (Figure 3). All the peaks of the major chromite phase are present in the coated sample along with the prominent peak of iron (Fe) from the substrate. Peaks related to quartz and hematite are present in both powder sample and coating, indicating that minerals did not undergo the decomposition process during deposition. The XRD pattern of coating shows no evidence of amorphous phases and the chromite phase remained crystalline in the as-sprayed form.

SEM was used to examine the microstructure of coatings. Micrographs of cross-section at different magnifications are shown in Figure 4a,b. Low magnification image Figure 4a of cross section shows a clear interface between the substrate and coating. Figure 4b reveals numerous pores and voids distributed throughout the coating cross-section with more concentration near the outer edge of the coating. The measured thickness values from micrographs revealed that, by using the fine powder, feedstock coating thickness of 64 ± 5 μm was produced, and for that of the coarse powder, thickness of 55 ± 6 μm was produced. Coating thicknesses were measured using calibrated scale bar of Olympus AnalySIS FIVE software.

Top surface morphology of both fine and coarse powder coating was rough, with fine powder coating having slightly less surface roughness than coarse powder coating (Table 5). It has been observed that minimum values of roughness average (Ra) recorded in both type of coatings come along the direction of passes of the deposition process and maximum values of Ra obtained were across the direction of passes (Table 5); this is because particles are more deformed at impact, along the direction of spray gum movement than other directions.[39] Porosity has been seen in coated samples, and measured values of percentage porosity are shown in Table 5. It has been observed that coatings exhibit higher percentages of porosity whether they were deposited by finer or coarse particles (Table 5). The porosity content is directly dependent on the melting of particles during the deposition process which indicates that some particles got completely melted during the spraying process.[40] The temperature and velocity of the particles during spraying, is directly dependent on the size of particles and it has been observed that very small particles tend to be heated more due to higher per unit surface area than larger particles.[41] To obtain smooth surfaces and a uniform microstructure, small particles with narrow size distribution will be favorable and they might produce thicker coatings at the cost of higher porosities in APS processes.[42] Values of microhardness of both coatings are shown in Table 5. Coatings exhibited higher hardness than the substrate material. Microhardness of fine particle coating is relatively higher than the coarse particles coating, as the coating is more compact due to the slightly lower porosity value than its counterpart.[43]

Voids and pores are present in both type of coatings and are clearly marked in coating top surface images (Figure 5a,b. The voids may be formed either due to the combination of some porosities or due to the shrinkage upon solidification (Figure 5b). Some unmelted particles placed at top surface of coarse powder coating were pointed out in Figure 5a. It is also suggested that the incomplete melting of some of the chromite powder could have contributed to the rougher coating surfaces. This can be explained by assuming that large powder particles were not melted entirely during the APS thermal spraying process instead partially melted and deformed at impact to the

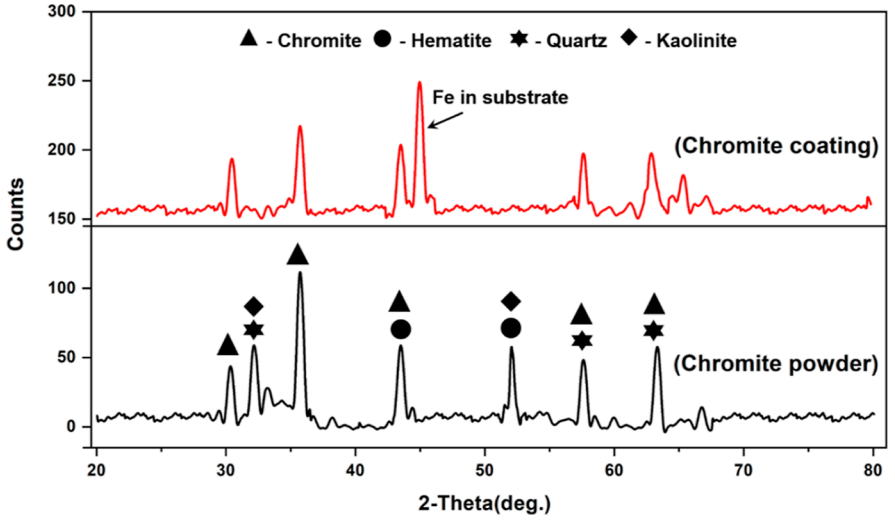

Figure 3. XRD graph of chromite powder and the coated sample.

https://doi.org/10.1021/acsomega.3c00194
ACS Omega 2023, 8, 15193−15202

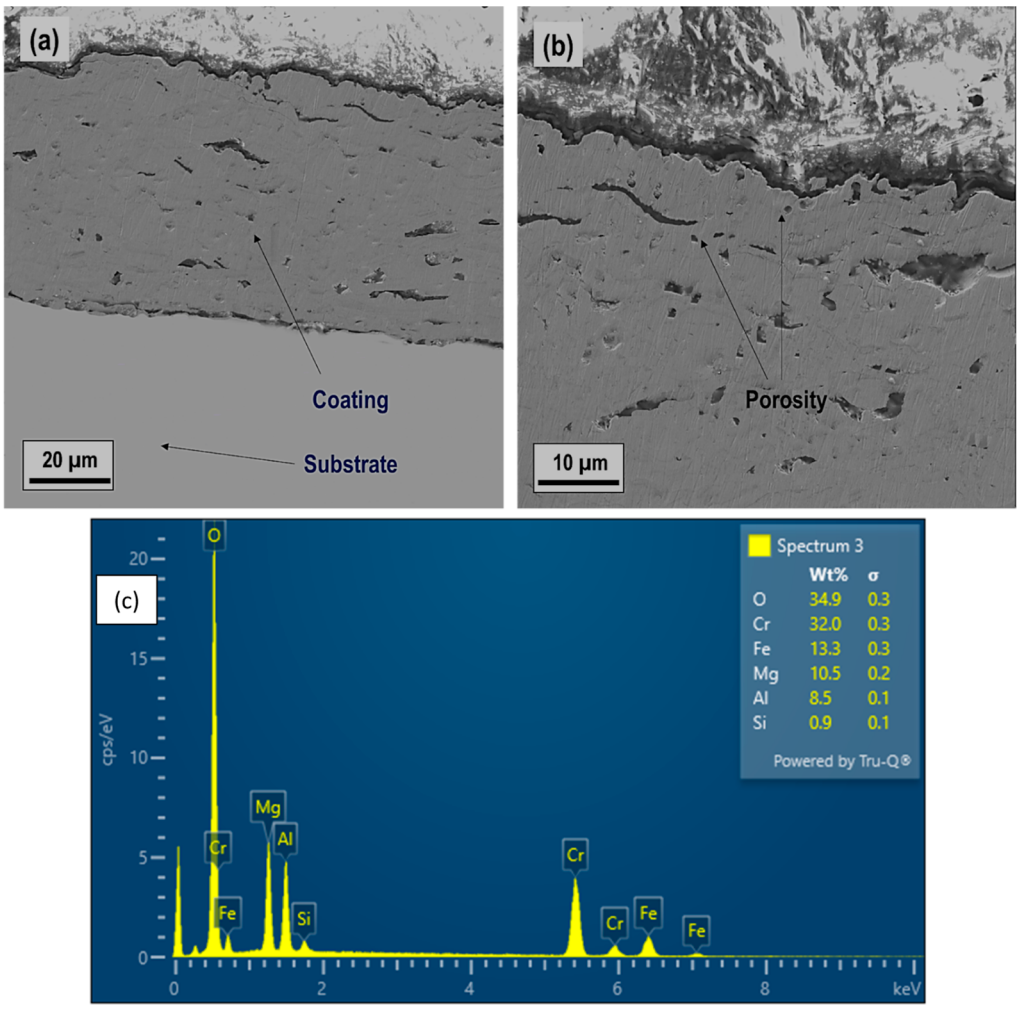

Figure 4. SEM image of cross-section of coatings (a) at low magnifications, (b) higher magnification, and (C) EDS scan.

Table 5. Porosity Content and Microhardness Values of Coatings

coating type	porosity (%)	hardness (HV)	roughness average Ra (μm)
coarse particle coating	11.3 ± 2	288 ± 8	2.5−3.1
fine particles coating	10.4 ± 2	297 ± 6	2.1−2.7

substrate. This was also the reason that fine particles were deposited more efficiently, having higher coating thickness with same spraying parameters as coarse particles.[44] Elemental area scan (EDS) taken from top surface of coating shows distribution of main elements in the coating surface (Figure 5). Even distribution of oxygen (O) along with chromium (Cr), iron (Fe), aluminum (Al), and magnesium (Mg) reveals the intrinsic oxide content of chromite mineral. Some silicon (Si) is also seen whose oxide form quartz mineral is present in powder and coating, as evident from XRD results. Quartz mineral resides as an impurity with the chromite mineral.

3.3. Tribological Properties. Sliding wear test of coating was examined on a ball-on-disk arrangement. As no prior data are available for the wear test of chromite coatings, therefore small values of loads were used to avoid exposing the substrate surface. Wear tests of both fine and coarse particle coatings and substrate were performed using two applied loads of 4 and 8 N for a total sliding distance of 50 m. Wear resistance of coatings was calculated in terms of specific wear rate formula which is as follows.[45]

$$K = \frac{V}{w.\ s}$$

K is specific wear rate (mm^3/Nm), V is the cumulative wear volume (mm^3), w is the normal load (N), and s is the sliding distance (m).

Table 6 shows that the specific wear rate of coatings made with the coarse feedstock powder has a higher specific wear rate as compared to coatings made by fine powder feedstock. Results (Table 6 and Figure 6) indicate that fine powder coatings are more wear resistant in both load conditions than coarse powder coatings which is in agreement with hardness values of both coatings, these results can also be anticipated from hardness values of fine and coarse particle coatings. Coatings exhibit higher hardness and wear resistance values than substrate that depicts their potential for wear resistance applications. For potential use in wear resistance applications, we should use small size and narrow distribution of particles that could lead to better and compact coatings. Lower surface roughness in the case of fine powder coating corresponds to decreased amount of fracture of surface asperities that results in lower wear volume and wear rate.[46] In our case the spread, shape, and size of particles determine wear properties, as the

https://doi.org/10.1021/acsomega.3c00194
ACS Omega 2023, 8, 15193−15202

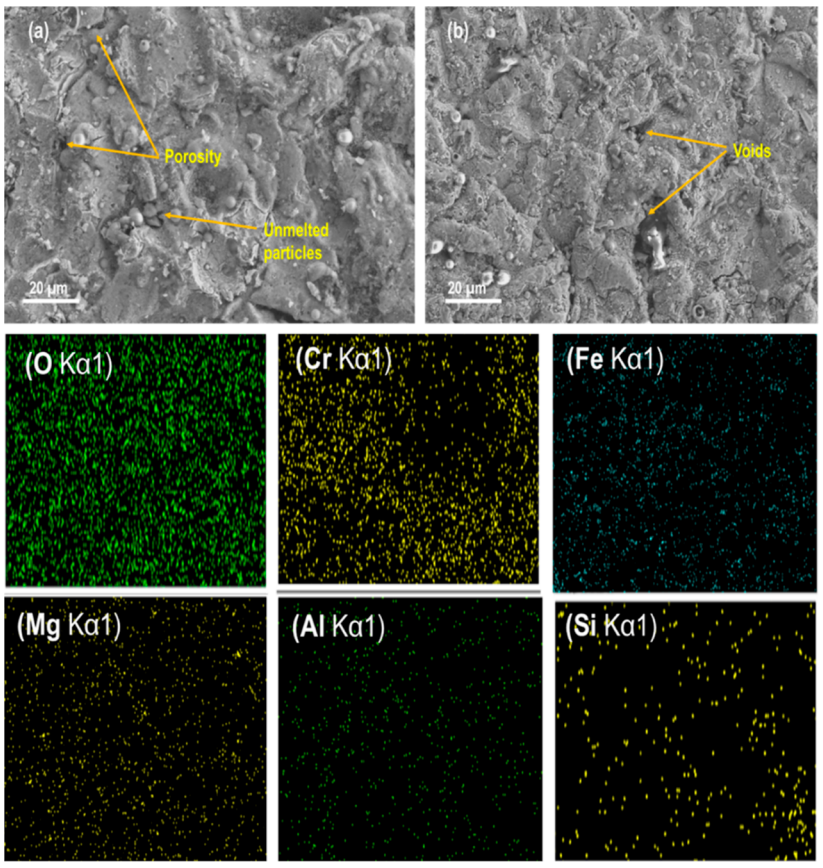

Figure 5. SEM image of the top surface of coarse powder coating (a) and fine powder coating (b) along with EDS mapping of elements from the top surface of fine particles coatings.

Table 6. Tribological Properties of the Coatings

coating	applied load (N)	accumulative wear volume (mm3)	specific wear rate ($mm^3\ N^{-1}m^{-1}$)	average COF
steel substrate	4	2.17 ± 0.18	10.85×10^{-3}	0.41
	8	4.42 ± 0.20	11.05×10^{-3}	0.40
coarse powder coating	4	1.02 ± 0.15	5.10×10^{-3}	0.36
	8	2.21 ± 0.17	5.52×10^{-3}	0.36
fine powder coating	4	0.97 ± 0.15	4.85×10^{-3}	0.35
	8	2.18 ± 0.18	5.45×10^{-3}	0.34

wear rate is sensitive to abrasive characteristics because wear rate increases with an increase in the coating roughness.[47]

Wear volume values shows that fine powder coating has relatively lower cumulative wear volume in applied load conditions of 4 and 8 N (Table 6), whereas coarse powder coatings have relatively higher cumulative wear volumes generated during the wear test. Relatively higher surface roughness and large uneven size distributed particles are the main cause of high wear rates and volumes of coarse powder coating because large particles pull out, causing more weight loss than small particles.[48] Large surface asperities are more deformed during sliding at higher loads, as seen in Figure 7d−f. Sometimes a bigger particle is ploughed away from the coatings and stays between the ball and grove area, increasing the material removal due to both rubbing and rolling actions also known as three body abrasion. Wear of coatings is dominated by ploughing as evident from wear debris particles

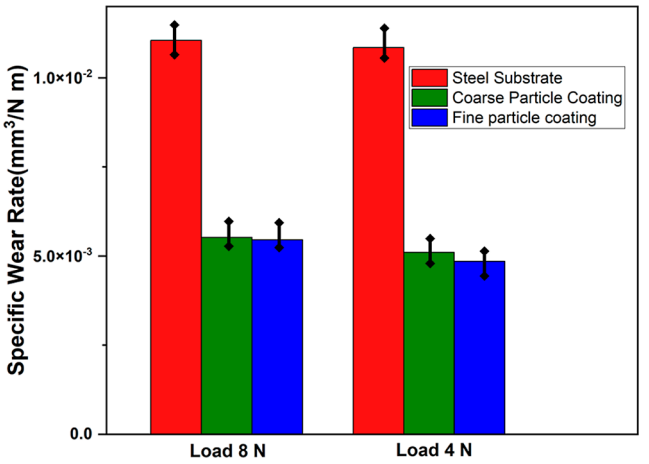

Figure 6. Wear rates of substrate and coatings done by fine and coarse particles under different load conditions.

present on the wear track (pointed in Figure 7c,e), and particle pull out and abrasive wear features can be seen in Figure 7c,f, which suggests coating is worn by abrasive wear.[49]

Wear tracks of both coatings were observed by SEM to analyze the wear mechanism and wear debris, see Figure 7. Wear track width of coatings are in agreement with wear volumes and no macroscopic cracks were observed in both type of coatings (Figure 7a,d). Fine debris of particles were also found around the wear tracks that suggest the fine particles pull out by scratching, which supports the phenomenon of wear by the abrasion mechanism.[50] To ensure the integrity of

https://doi.org/10.1021/acsomega.3c00194
ACS Omega 2023, 8, 15193−15202

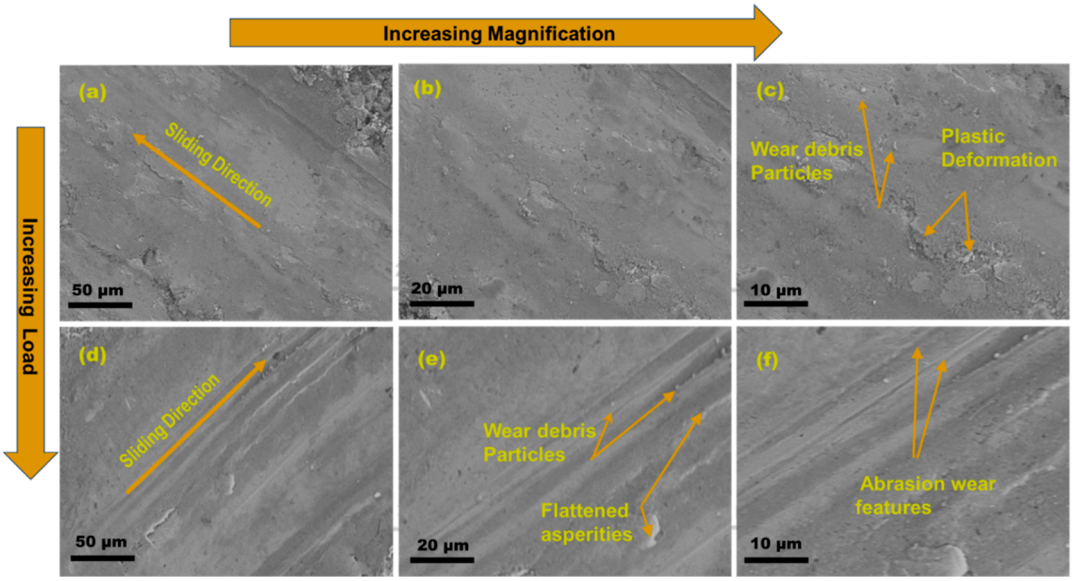

Figure 7. SEM micrographs of worn surfaces of chromite coating under 4 N load condition with successive magnifications (a–c) and at 8 N load with successive magnifications (d–f).

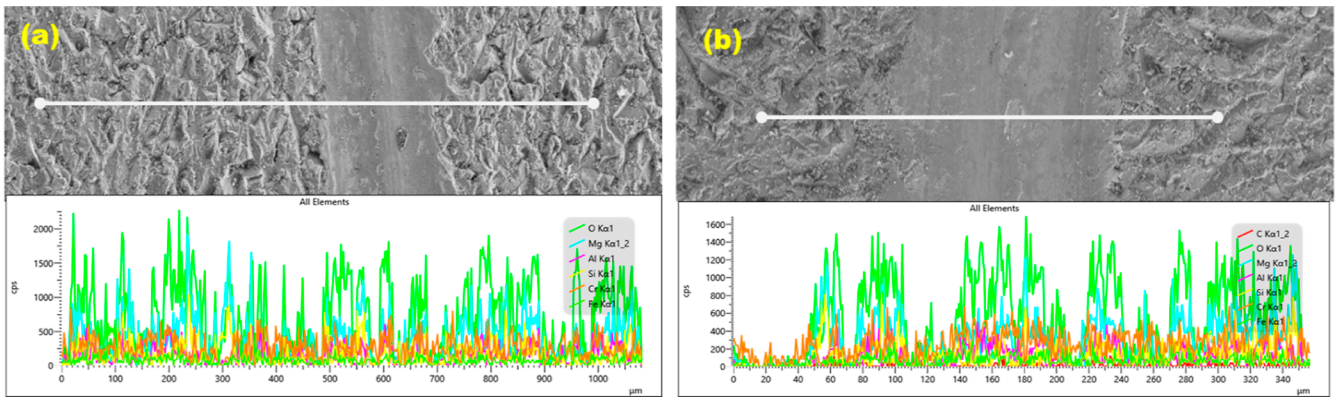

Figure 8. EDS line scan over worn surface of 4 N applied load (a) and with 8 N applied load (b).

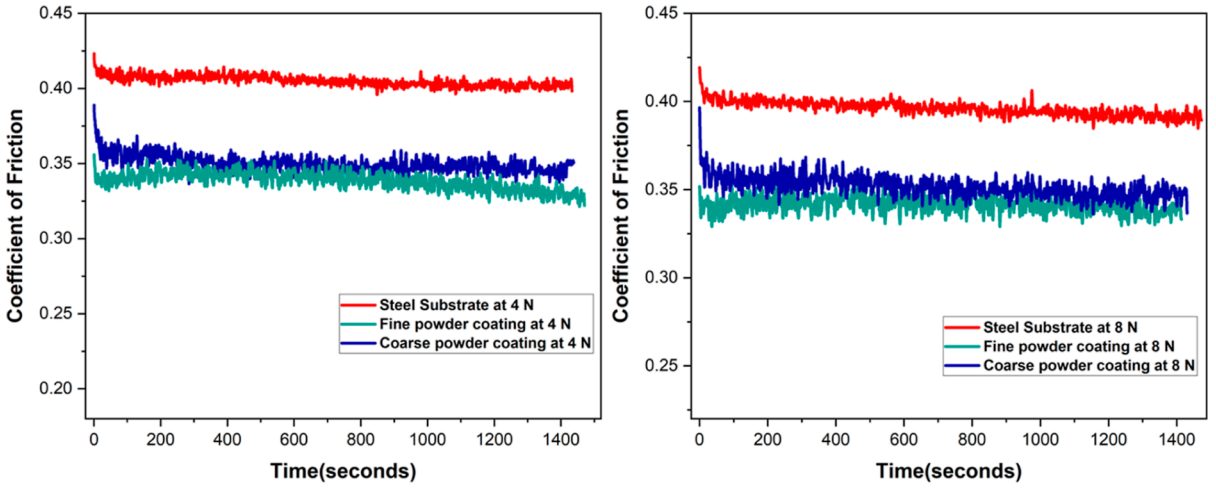

Figure 9. Friction coefficient of substrate and coatings and under different load conditions.

coating after wear and friction test, EDS line scan was taken over the worn surface. It can be seen in Figure 8 that the line scan started from unworn area and ended at unworn area after passing through the worn area. The variation of coating elements can be seen over the range of area. Line scans revealed that wear tracks show no sign of exposure to substrate surface in both load conditions which indicate that the integrity of the coating is intact.

https://doi.org/10.1021/acsomega.3c00194
ACS Omega 2023, 8, 15193−15202

Coefficient of friction (COF) of the coatings were measured on both load conditions and graphs were drawn between COF and elapsed time during the wear test, see Figure 9. Temporary running-in stage in the beginning of friction curves was observed in all cases. It can be seen that as coatings have more hardness than the substrate, therefore their COF values are little lower than the substrate which is in agreement with the literature. Fine powder coatings and substrate have shown lower COF values at higher applied loads which indicates that the frictional force does not increased in proportion to applied load which resulted in decreased COF upon increasing normal load values.[51−53] In general, COF values decrease with the decrease in surface roughness that is why coarse particle coating displays large values of COF as compared to fine particle coating (Figure 9). Surface texture plays a vital role in determining COF as in our case both unmelted particles and pores were present in coarse and fine particle coatings, respectively.[54] Texture was more rough in coarse particle coating, uneven shape larger particles, and voids were creating hindrance to sliding abrasion and thus causing higher COF values and noise.[46,55]

3.4. Corrosion Behavior. Results of potentiodynamic polarization measurements carried out on samples are shown in Figure 10. Corrosion current density and corrosion rates

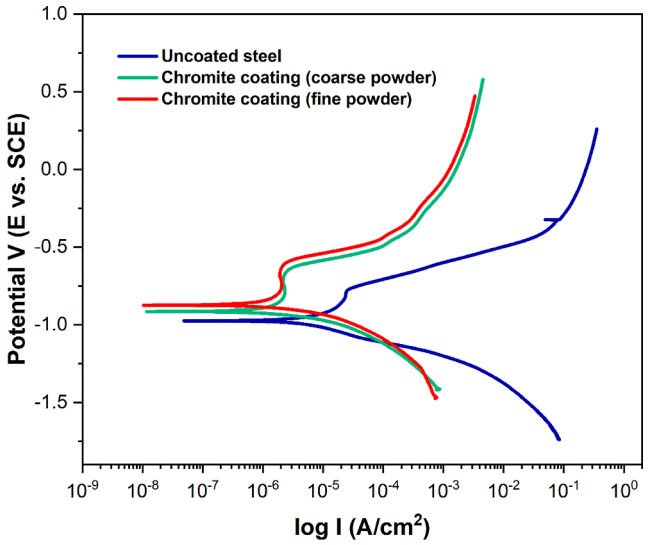

Figure 10. Tafel curves of mild steel substrate and chromite coatings.

were measured by employing the Tafel fit on polarization curves using Gamry Echem analyst software. Resulting values are given in Table 7 for which 120 mV straight line portion of anodic and cathodic branch were used by software. Fine powder coating has least corrosion rate of 1.1 mpy (mils per year) in comparison with coarse particle coating (1.2 mpy). These corrosion rates are one-fourth of the rate of bare metal. These results show that chromite coatings applied by the APS technique exhibit good corrosion resistance in comparison to mild steel substrate. The polarization curves show that chromite coatings display relatively noble corrosion potential than bare metal. Fine powder coating shows more noble potential than coating deposited by coarse particles and this can be explained by the presence of relatively higher surface area for chemical reaction due to higher percentage of porosity in coarse particle coating.[32] Presence of inhomogeneities such as voids and pores on the passive oxide layer (coating surface) favor the pitting corrosion by the formation of localized cells during corrosion reaction, as corrosion rate increases with defect density on the surface.[56] Oxides present in coating are thermodynamically stable due to their natural existence in low energy state. As corrosion drive from metal to metal-oxide and from unstable to stable metal oxide, the order of stability of metal oxides realized from Gibbs free energy will be MgO > Al_2O_3 > Cr_2O_3 > Fe_2O_3. Initial part of anodic branch in Tafel plot shows a very small change in current density values up to −550 mV that may correspond to more stable passive oxides (chromite), whereas higher change in current density at the end of anodic branch from −300 to 500 mV may corresponds to less stable oxide like hematite (Fe_2O_3). The region between −550 and 300 mV corresponds to the passive−active transition zone, where defect density plays a vital role. Anodic branch of the Tafel plot shows passivation that occurred at the surface of coating due to the presence of the chromite phase, evidence of Cr_2O_3 performance as a passive film was reported elsewhere.[34,57] The presence of stable phases in chromite coating, makes it an excellent candidate for future applications related to corrosion resistance properties.

Table 7. Electrochemical Corrosion Data for Substrates and Coatings

material	corrosion potential E_{corr} (mV)	corrosion current density I_{corr} (µ A/cm^2)	corrosion rate (mpy)
substrate	−982	9.7	4.5
coarse particle coating	−903	2.67	1.2
fine particles coating	−865	2.31	1.1

4. CONCLUSIONS

No prior studies and reference data are available for chromite mineral coatings; however, following conclusions can be drawn from our experiments and characterizations.

- Metallurgical grade natural chromite can be used as a coating material for the APS technique after concentration and proper comminution to few μm size.
- Chromite powder of two different size ranges have been deposited by the APS technique to form coatings on mild steel substrates. The coating deposition efficiency of fine powder was better than coarse powder during thermal spraying, as the coating thickness of fine powder was greater than coarse powder using same parameters.
- Wear behavior of fine powder coating was better than coarse powder coating as evident from specific wear rates and hardness values. Whereas coefficient of friction values for both fine and coarse particle coatings are fairly close with a small advantage for fine particle coatings. Chromite coating can be safely used as a potential candidate for abrasion resistance applications.
- Chromite coating has provided sufficient corrosion protection to a mild steel substrate; therefore, natural chromite coating can be used as an economical solution to the corrosion protection of carbon steels as compared to its synthetic counterparts.

https://doi.org/10.1021/acsomega.3c00194
ACS Omega 2023, 8, 15193−15202

ETHICS APPROVAL

All authors confirm that they follow all ethical guidelines. All authors certify that they have no affiliations with or involvement in any organization or entity with any financial interest or non-financial interest in the subject matter or materials discussed in this paper.

AUTHOR INFORMATION

Corresponding Authors

Muhammad Atiq Ur Rehman − *Materials Science and Engineering Department, Institute of Space Technology, 44000 Islamabad, Pakistan;* orcid.org/0000-0001-5201-973X; Email: atique1.1@hotmail.com

Akbar Niaz − *Department of Mechanical Engineering, King Faisal University, Al Hufūf 31982, Saudi Arabia;* Email: abutt@kfu.edu.sa

Authors

Zeeshan Ahmad Abbasi − *Materials Science and Engineering Department, Institute of Space Technology, 44000 Islamabad, Pakistan*

Abdul Mateen − *Materials Science and Engineering Department, Institute of Space Technology, 44000 Islamabad, Pakistan*

Abdul Wadood − *Materials Science and Engineering Department, Institute of Space Technology, 44000 Islamabad, Pakistan*

Complete contact information is available at: https://pubs.acs.org/10.1021/acsomega.3c00194

Author Contributions

The authors' contributions are as follows: Z. conceptualized, planned, and carried out the experiments. M.A.R. contributed to the analysis and interpretation of results. A.W. and A.M. validated, prepared, and edited the original draft, supervised, and critically reviewed the research and manuscript. All the authors provided valuable feedback and helped to shape the project, analysis, and the manuscript.

Funding

This research work was partially funded by the Institute of Space technology Islamabad, Pakistan.

Notes

The authors declare no competing financial interest.

The data presented and/or analyzed during the current study are available from the corresponding author on request.

ACKNOWLEDGMENTS

This work was supported by the Deanship of Scientific Research, Vice Presidency for Graduate Studies and Scientific Research, King Faisal University, Saudi Arabia [Project no. GRANT2604].

REFERENCES

(1) Ctibor, P.; Nevrlá, B.; Pala, Z.; Vrtiaka, L. Natural Tourmaline as an Efficient Alternative to Ceramic-Type Material for Plasma Spraying. *J. South. Afr. Inst. Min. Metall. scieloza* **2018**, 387−393.

(2) Bhuyan, S. K.; Thiyagarajan, T. K.; Mishra, S. C. Development of Ceramic Coating on Metal Substrate Using Industrial Waste and Ore Mineralstle. *Mater. Sci. Eng. Conf. Ser.* **2017**, *178*, 12029.

(3) Karhu, M.; Lagerbom, J.; Honkanen, M.; Huttunen-Saarivirta, E.; Kiilakoski, J.; Vuoristo, P.; Solismaa, S.; Kivikytö-Reponen, P. Mining Tailings as a Raw Material for Glass-Bonded Thermally Sprayed Ceramic Coatings: Microstructure and Properties. *J. Eur. Ceram. Soc.* **2020**, *40*, 4111−4121.

(4) Pham, D. Q.; Berndt, C. C.; Gbureck, U.; Zreiqat, H.; Truong, V. K.; Ang, A. S. M. Mechanical and Chemical Properties of Baghdadite Coatings Manufactured by Atmospheric Plasma Spraying. *Surf. Coat. Technol.* **2019**, *378*, 124945.

(5) Ctibor, P.; Sedláček, J.; Straka, L. *Dielectric Properties of Plasma-Sprayed Fully Natural Garnets. Coatings*, 2022.

(6) Ratha, I.; Datta, P.; Balla, V. K.; Nandi, S. K.; Kundu, B. Effect of Doping in Hydroxyapatite as Coating Material on Biomedical Implants by Plasma Spraying Method: A Review. *Ceram. Int.* **2021**, *47*, 4426−4445.

(7) Ctibor, P.; Nevrlá, B.; Neufuss, K.; Petrášek, J. . S.; Sedláček, J. Plasma Spray Coatings of Natural Ores From Structural, Mechanical, Thermal, and Dielectric Viewpoints. *Coatings* **2019**, *10*, 3.

(8) Ctibor, P.; Nevrla, B.; Pala, Z.; Sedlacek, J.; Soumar, J.; Kubatik, T.; Neufuss, K.; Vilemova, M.; Medricky, J. Study on the Plasma Sprayed Amorphous Diopside and Annealed Fine-Grained Crystalline Diopside. *Ceram. Int.* **2015**, *41*, 10578−10586 Part A).

(9) Samadi, H.; Pershin, L.; Coyle, T. W. Effect of In-Flight Particle Properties on Deposition of Air Plasma Sprayed Forsterite. *Surf. Coat. Technol.* **2010**, *204*, 3300−3306.

(10) Arnold, D. Ceramic Theory and Cultural Process after 25 Years. *Ethnoarchaeology* **2011**, *3*, 63−98.

(11) Salman, S.; Köse, R.; Urtekin, L.; Findik, F. An Investigation of Different Ceramic Coating Thermal Properties. *Mater. Des.* **2006**, *27*, 585−590.

(12) Liu, Y.; Fischer, T. E.; Dent, A. Comparison of HVOF and Plasma-Sprayed Alumina/Titania Coatings—Microstructure, Mechanical Properties and Abrasion Behavior. *Surf. Coat. Technol.* **2003**, *167*, 68−76.

(13) Matikainen, V.; Niemi, K.; Koivuluoto, H.; Vuoristo, P. *Abrasion, Erosion and Cavitation Erosion Wear Properties of Thermally Sprayed Alumina Based Coatings*, 2014.

(14) Fauchais, P. L.; Heberlein, J. V. R.; Boulos, M. I. D. C.. In *Plasma Spraying BT - Thermal Spray Fundamentals: From Powder to Part*; Fauchais, P. L., Heberlein, J. V. R., Boulos, M. I., Eds.; Springer US: Boston, MA, 2014, pp 383−477.

(15) Mauer, G.; Vaßen, R.; Stöver, D. Plasma and Particle Temperature Measurements in Thermal Spray: Approaches and Applications. *J. Therm. Spray Technol.* **2011**, *20*, 391−406.

(16) Li, M.; Christofides, P. D. Computational Study of Particle In-Flight Behavior in the HVOF Thermal Spray Process. *Chem. Eng. Sci.* **2006**, *61*, 6540−6552.

(17) Li, M.; Christofides, P. D. Modeling and Analysis of HVOF Thermal Spray Process Accounting for Powder Size Distribution. *Chem. Eng. Sci.* **2003**, *58*, 849−857.

(18) Houdková, Š.; Kašparová, M.; Zahálka, F. The Influence of Spraying Angle on Properties of HVOF Sprayed Hardmetal Coatings. *J. Therm. Spray Technol.* **2010**, *19*, 893−901.

(19) Stevens, R. E. Composition of Some Chromites of the Western Hemisphere. *Am. Mineral.* **1944**, *29*, 1−34.

(20) Murthy, Y. R.; Tripathy, S. K.; Kumar, C. R. Chrome Ore Beneficiation Challenges & Opportunities − A Review. *Miner. Eng.* **2011**, *24*, 375−380.

(21) Koleli, N.; Demir, A.. In *Chapter 11 - Chromite*; Prasad, M. N. V., Shih, K. B. T.-E. M., Eds.; Academic Press, 2016, pp 245−263.

(22) Pilchin, A.; Eppelbaum, L. Concentration of Platinum Group Elements During the Early Earth Evolution: A Review. *Nat. Resour.* **2017**, *08*, 172−233.

(23) Hong, Q.-J.; Ushakov, S. V.; van de Walle, A.; Navrotsky, A. Melting Temperature Prediction Using a Graph Neural Network Model: From Ancient Minerals to New Materials. *Proc. Natl. Acad. Sci. U.S.A.* **2022**, *119*, No. e2209630119.

(24) Sánchez-Ramos, S.; Doménech-Carbó, A.; Gimeno-Adelantado, J. V.; Peris-Vicente, J. Analytical and Mineralogical Studies of Ore and Impurities from a Chromite Mineral Using X-Ray Analysis, Electrochemical and Microscopy Techniques. *Talanta* **2008**, *74*, 1592−1597.

(25) Öztürk, F. D.; Abakay Temel, H. Beneficiation of Konya-Beyşehir Chromite for Producing Concentrates Suitable for Industry. *JOM* **2016**, *68*, 2449−2454.
(26) Bolelli, G.; Steduto, D.; Kiilakoski, J.; Varis, T.; Lusvarghi, L.; Vuoristo, P. Tribological Properties of Plasma Sprayed Cr2O3, Cr2O3−TiO2, Cr2O3−Al2O3 and Cr2O3−ZrO2 Coatings. *Wear* **2021**, *480*−*481*, 203931.
(27) Yang, X.; Zeng, J.; Zhang, H.; Wang, J.; Sun, J.; Dong, S.; Jiang, J.; Deng, L.; Zhou, X.; Cao, X. Correlation between Microstructure, Chemical Components and Tribological Properties of Plasma-Sprayed Cr2O3-Based Coatings. *Ceram. Int.* **2018**, *44*, 10154−10168.
(28) Gerald, O. J.; Wenge, L.; Yuan Tao, Z.; Cheng Long, L.; Qiang, L. Influence of Plasma Spraying Current on the Microstructural Characteristics and Tribological Behaviour of Plasma Sprayed Cr2O3 Coating. *Boletin la Soc. Española Cerámica y Vidr.* **2021**, *60*, 338−346.
(29) Zamani, P.; Valefi, Z. Microstructure, Phase Composition and Mechanical Properties of Plasma Sprayed Al2O3, Cr2O3 and Cr2O3-Al2O3 Composite Coatings. *Surf. Coat. Technol.* **2017**, *316*, 138−145.
(30) Akram, W.; Mateen, A.; Qazi, I.; Hussain, A. Development and Characterization of Cost Effective Wear and Corrosion Resistant HVOF Sprayed Chromite Coatings and Hard Chrome Plating *16th International Bhurban Conference on Applied Sciences and Technology (IBCAST)*; IEEE, 2019; pp 66−73.
(31) Oje, A. M.; Ogwu, A. A.; Rahman, S. U.; Oje, A. I.; Tsendzughul, N. Effect of Temperature Variation on the Corrosion Behaviour and Semiconducting Properties of the Passive Film Formed on Chromium Oxide Coatings Exposed to Saline Solution. *Corros. Sci.* **2019**, *154*, 28−35.
(32) Zamani, P.; Valefi, Z.; Jafarzadeh, K. Comprehensive Study on Corrosion Protection Properties of Al2O3, Cr2O3 and Al2O3−Cr2O3 Ceramic Coatings Deposited by Plasma Spraying on Carbon Steel. *Ceram. Int.* **2022**, *48*, 1574−1588.
(33) Tripathy, S. K.; Banerjee, P. K.; Suresh, N. Magnetic Separation Studies on Ferruginous Chromite Fine to Enhance Cr:Fe Ratio. *Int. J. Miner. Metall. Mater.* **2015**, *22*, 217−224.
(34) Samal, S. K.; Mohanty, M. K.; Mishra, B.; Mishra, S. C. Thermal Transformation of Oxide and Hydroxide Minerals in Chromite and Manganese Ores. *Min. Metall. Explor.* **2021**, *38*, 1125−1134.
(35) Mohan, R.; Deevakar, L.; Sivakumar, V. Towards Holistic Technology Solution to Chromite Ore Processing Residue (COPR) Challenge; Global Issue: Review and Analysis. *Int. J. Environ. Sci. Technol.* **2022**, *19*, 665−676.
(36) Zhou, M.-F.; Robinson, P. T.; Su, B.-X.; Gao, J.-F.; Li, J.-W.; Yang, J.-S.; Malpas, J. Compositions of Chromite, Associated Minerals, and Parental Magmas of Podiform Chromite Deposits: The Role of Slab Contamination of Asthenospheric Melts in Suprasubduction Zone Environments. *Gondwana Res* **2014**, *26*, 262−283.
(37) Meher, K. R. S. P.; Martin, C.; Caignaert, V.; Damay, F.; Maignan, A. Multiferroics and Magnetoelectrics: A Comparison between Some Chromites and Cobaltites. *Chem. Mater.* **2014**, *26*, 830−836.
(38) Tang, D.; Qin, K.; Evans, N. J.; Fang, L. Silicate Mineral Inclusions in Chromite from the Eastern Bushveld Complex: Implications for the Origin and Evolution of Hydrous Melt during Chromite Mineralization in the Critical Zone. *Lithos* **2023**, *438*−*439*, 106997.
(39) Ganvir, A.; Calinas, R. F.; Markocsan, N.; Curry, N.; Joshi, S. Experimental Visualization of Microstructure Evolution during Suspension Plasma Spraying of Thermal Barrier Coatings. *J. Eur. Ceram. Soc.* **2019**, *39*, 470−481.
(40) Hashemi, S. M.; Parvin, N.; Valefi, Z.; Alishahi, M. Comparative Study on Tribological and Corrosion Protection Properties of Plasma Sprayed Cr2O3-YSZ-SiC Ceramic Coatings. *Ceram. Int.* **2019**, *45*, 21108−21119.
(41) Cho, T. Y.; Yoon, J. H.; Yoon, S. H.; Joo, Y. K.; Choi, W. H.; Son, Y. B. The Effects of Particle Size on the Surface Properties of an HVOF Coating of WC-Co. *Korean J. Met. Mater.* **2017**, *55*, 227−231.
(42) Oksa, M.; Turunen, E.; Suhonen, T.; Varis, T.; Hannula, S.-P. *Optimization and Characterization of High Velocity Oxy-Fuel Sprayed Coatings: Techniques, Materials, and Applications*, 2011.
(43) WANG, D.; ZHANG, B.; JIA, C.; GAO, F.; YU, Y.; ZHAO, X.; BAI, Z. Microstructure and Tribological Properties of Plasma-Sprayed WC-17 Co Coatings with Different Carbide Grain Size Distribution. *J. Jpn. Soc. Powder Powder Metall.* **2016**, *63*, 688−696.
(44) Fauchais, P.; Montavon, G.; Bertrand, G. From Powders to Thermally Sprayed Coatings. *J. Therm. Spray Technol.* **2010**, *19*, 56−80.
(45) Holmberg, K.; Matthews, A. *Coatings Tribology: Properties, Mechanisms, Techniques and Applications in Surface Engineering*, 2nd Editio.; Elsevier Science, 2009.
(46) Karaoglanli, A. C.; Oge, M.; Doleker, K. M.; Hotamis, M. Comparison of Tribological Properties of HVOF Sprayed Coatings with Different Composition. *Surf. Coat. Technol.* **2017**, *318*, 299−308.
(47) Federici, M.; Menapace, C.; Moscatelli, A.; Gialanella, S.; Straffelini, G. Effect of Roughness on the Wear Behavior of HVOF Coatings Dry Sliding against a Friction Material. *Wear* **2016**, *368*−*369*, 326−334.
(48) Jiang, X.-Y.; Hu, J.; Jiang, S.-L.; Wang, X.; Zhang, L.-B.; Li, Q.; Lu, H.-P.; Yin, L.-J.; Xie, J.-L.; Deng, L.-J. Effect of High-Enthalpy Atmospheric Plasma Spraying Parameters on the Mechanical and Wear Resistant Properties of Alumina Ceramic Coatings. *Surf. Coat. Technol.* **2021**, *418*, 127193.
(49) Pulsford, J.; Kamnis, S.; Murray, J.; Bai, M.; Hussain, T. Effect of Particle and Carbide Grain Sizes on a HVOAF WC-Co-Cr Coating for the Future Application on Internal Surfaces: Microstructure and Wear. *J. Therm. Spray Technol.* **2018**, *27*, 207−219.
(50) Sahraoui, T.; Fenineche, N. E.; Montavon, G.; Coddet, C. Structure and Wear Behaviour of HVOF Sprayed Cr3C2-NiCr and WC-Co Coatings. *Mater. Des.* **2003**, *24*, 309−313.
(51) Chowdhury, M.; Nuruzzaman, D. M.; Mia, A. H.; Rahaman, M. Friction Coefficient of Different Material Pairs Under Different Normal Loads and Sliding Velocities. *Tribol. Ind.* **2012**, *34*, 18−23.
(52) Autay, R.; Kchaou, M.; Dammak, F. Friction and Wear Behavior of Steels under Different Reciprocating Sliding Conditions. *Tribol. Trans.* **2012**, *55*, 590−598.
(53) Chowdhury, M. A.; Khalil, M. K.; Nuruzzaman, D. M.; Rahaman, M. L. The Effect of Sliding Speed and Normal Load on Friction and Wear Property of Aluminum. *Int. J. Mech. Mech. Eng.* **2011**, *11*, 53−57.
(54) Odhiambo, J. G.; Li, W.; Zhao, Y.; Li, C. *Porosity and Its Significance in Plasma-Sprayed Coatings*, 2019.
(55) Svahn, F.; Kassman-Rudolphi, Å.; Wallén, E. The Influence of Surface Roughness on Friction and Wear of Machine Element Coatings. *Wear* **2003**, *254*, 1092−1098.
(56) Galedari, S. A.; Mahdavi, A.; Azarmi, F.; Huang, Y.; McDonald, A. A Comprehensive Review of Corrosion Resistance of Thermally-Sprayed and Thermally-Diffused Protective Coatings on Steel Structures. *J. Therm. Spray Technol.* **2019**, *28*, 645−677.
(57) Babu, P. S.; Sen, D.; Jyothirmayi, A.; Krishna, L. R.; Rao, D. S. Influence of Microstructure on the Wear and Corrosion Behavior of Detonation Sprayed Cr2O3-Al2O3 and Plasma Sprayed Cr2O3 Coatings. *Ceram. Int.* **2018**, *44*, 2351−2357.

https://doi.org/10.1021/acsomega.3c00194
ACS Omega 2023, 8, 15193−15202